Strong ferromagnetism induced by canted antiferromagnetic order in double perovskite iridates (La_{1−x}Sr_{x})_{2}ZnIrO_{6}

W. K. Zhu, Chi-Ken Lu, W. Tong, J. M. Wang, H. D. Zhou, and S. X. Zhang

Strong 'ferromagnetism' induced by canted antiferromagnetic order in double perovskite iridates $(La_{1-x}Sr_x)_2ZnIrO_6$

W. K. Zhu,[1] Chi-Ken Lu,[2] W. Tong,[3] J. M. Wang,[1] H. D. Zhou,[4] and S. X. Zhang[1, *]

[1] *Department of Physics, Indiana University, Bloomington, IN 47405, USA*

[2] *Physics Department, National Taiwan Normal University, Taipei 11677, Taiwan*

[3] *High Magnetic Field Laboratory, Chinese Academy of Sciences, Hefei 230031, Anhui, China*

[4] *Department of Physics and Astronomy,*
University of Tennessee, Knoxville, TN 37996, USA

Abstract

Iridates represent a unique material system that possesses both strong spin-orbit coupling (SOC) and electron correlation. The interplay between SOC and correlation could facilitate the emergence of novel electronic and magnetic states. In this work, we report on a systematic study of magnetism in double perovskite iridate La_2ZnIrO_6 and its hole-doped compounds $(La_{1-x}Sr_x)_2ZnIrO_6$ via dc magnetization measurement, heat capacity characterization, electron spin resonance spectroscopy and simple modeling. The undoped La_2ZnIrO_6 undergoes two magnetic transitions at $T_1 \sim 7.3$ K and $T_2 \sim 8.5$ K, respectively. While magnetic hysteresis loops with large remnant moments were observed below these two transition temperatures, the corresponding magnetic states were demonstrated to be canted antiferromagnetism (AFM) by the linear increase of magnetization at high field along with the observation of antiferromagnetic resonance. The nature of the canted AFM states with large canting angles can be understood by a simple model that includes both the Heisenberg exchange interaction and the Dzyaloshinskii-Moriya interaction. With the introduction of Ir^{5+} by Sr^{2+} doping, the canted AFM phases are suppressed, accompanied by an enhancement of electrical conductivity.

PACS numbers: 75.60.-d, 75.30.Kz, 75.40.-s, 76.30.-v

I. INTRODUCTION

Iridates represent a unique material system that possesses strong spin-orbit coupling (SOC) with an energy scale comparable to electron correlations (U)[1–6]. The interplay and competition between SOC and correlations facilitate the emergence of novel quantum states such as the $J_{\text{eff}}=1/2$ Mott state[1,7–9], quantum spin liquid[10,11], topological Mott insulators[2,3,12], and Weyl semimetals[4,13]. The strength of SOC and correlation relative to electron hopping (t) is strongly dependent on the crystal structure. A representative system of enhanced correlation is the so-called double perovskite iridates with a chemical formula of A_2BIrO_6, where A = rare earth or alkaline earth element and B =3d transition metal element such as Zn. The electronically active Ir^{4+} ions are well separated from each other, giving rise to highly localized electronic states[6].

While there have been considerable work in exploring and understanding novel magnetic properties of other iridates (e.g. pyrochlores[14–20], honeycomb lattice[5,21–24], and perovskites[25–28]), the highly-localized double-perovskite A_2BIrO_6 are much less intensively studied[29–38] and their magnetic properties remains to be fully understood. Using the prototypical La_2ZnIrO_6 as an example, magnetic susceptibility measurement indicates a paramagnetic (PM) to ferromagnetic (FM) -like transition around 7.5 K[29,31], however, recent density functional theory (DFT) calculations suggest that the low temperature ground state should be canted antiferromagnetism (AFM) instead of ferromagnetic order[39]. Neutron scattering measurement indeed shows signature of canted AFM, although the obtained information is limited by the low scattering intensity due to the large neutron absorption cross section of Ir[39]. Temperature dependence of inverse susceptibility in the PM state deviates from the linear Curie-Weiss law, yielding different signs of Weiss constant Θ depending on the temperature range that was chosen for fitting[29,31,39]. The understanding of these unusual magnetic properties is expected to provide significant insight into the interplay and competition between various interactions[6].

In this paper, we report on a systematic study of magnetism in La_2ZnIrO_6 and its hole-doped compounds $(La_{1-x}Sr_x)_2ZnIrO_6$ via dc magnetization measurement, heat capacity characterization, electron spin resonance (ESR) spectroscopy and theoretical modeling. The undoped La_2ZnIrO_6 undergoes two magnetic transitions at $T_1 \sim 7.3$ K and $T_2 \sim 8.5$ K, respectively. The magnetic phases below these two transition temperatures are both canted

AFM with possibly different canting angles, as evidenced by the magnetic hysteresis loops and antiferromagnetic resonance. The nature of the canted AFM states and the temperature dependence of inverse susceptibility in the PM state can be understood by a simple model that includes both the Heisenberg exchange interaction and the Dzyaloshinskii-Moriya interaction. With the introduction of Ir^{5+} by Sr^{2+} doping, both canted AFM phases are suppressed, accompanied by an enhancement of electrical conductivity.

II.   EXPERIMENTAL METHODS

The $(La_{1-x}Sr_x)_2ZnIrO_6$ ($x = 0$, 0.1 and 0.2) samples were prepared by conventional solid state reaction. Mixtures of high purity La_2O_3 (99.999%, dry), $SrCO_3$ (99.994%), ZnO (99.999%) and IrO_2 (99.99%) in stoichiometric ratios were heated in air at temperatures between 900 °C and 1050 °C for about 5 days with several intermediate grindings. The structure was characterized by X-ray powder diffraction (XRD) using a PANalytical EMPYREAN diffractometer (Cu Kα radiation). Rietveld refinements were performed for the XRD data using the GSAS software package[40,41] (see Fig. S1 in the Supplemental Material[42]). The magnetization measurements were performed in a Quantum Design Magnetic Property Measurement System. The heat capacity measurements were carried out in a Quantum Design Physical Property Measurement System. The ESR spectra were taken in an X-band BRUKER EMX plus 10/12 spectrometer (microwave frequency $\nu = 9.40$ GHz). The resistivity was measured using a Linear Research LR-700 AC Resistance Bridge.

III.   RESULTS AND DISCUSSION

A.   Undoped La_2ZnIrO_6

The undoped La_2ZnIrO_6 undergoes two magnetic transitions at low temperatures. Figure 1(a) shows the magnetization as a function of temperature taken at $H = 1$ kOe after the sample was cooled down in zero field (i.e. zero field cooling: ZFC) and in a field of 1 kOe (i.e. field cooling: FC). The magnetization increases gradually with the decrease of temperature down to about 10 K, below which it increases sharply and a ferromagnetic-like hysteresis between ZFC and FC is observed. The FC dM/dT versus T curve [inset of Fig. 1(a)] shows a major dip at $T_1 \sim 7.3$ K and a minor one at $T_2 \sim 8.5$ K, suggesting two magnetic phase

transitions. These two transitions become clearer in the magnetization data taken at lower magnetic fields [Fig. 1(b)]. The lower transition temperature of 7.3 K is close to the value determined by the Arrott analysis[39]. The ZFC M-T curves exhibit two peaks which should be attributed to the freezing of magnetic domains at low temperatures, as evidenced by the increase of peak temperatures with the decrease of applied magnetic field [dashed lines in Fig. 1(b)].

The existence of two magnetic transitions is further confirmed by temperature (T) dependent heat capacity (C_p) measurement. As shown in Fig. 2(a) and its inset, the heat capacity shows two peaks around T_1 and T_2. By subtracting the contribution from lattice that is represented by the heat capacity of the non-magnetic La_2ZnTiO_6, we obtained the magnetic specific heat ΔC_p and the magnetic entropy $S = \int \Delta C_p/T dT$. As seen in Fig. 2(b), the entropy is released after magnetic transitions by ~ 5.92 J/mol K, which is close to $R\ln 2 = 5.76$ J/mol K expected for the ordering of J_{eff}=1/2 moments[43]. We note that the magnetic specific heat is positive well above T_2, as also observed in previous study[39]. This positive magnetic specific heat may arise from a short-range ordered magnetic state that will be discussed below.

Magnetization versus magnetic field $(M$-$H)$ measurement was performed at several temperatures to understand the magnetic phases in different temperature regimes. When the temperature is below $T_2 \sim 8.5$ K, small magnetic hysteresis loops were observed at low fields, accompanied by a linear-like increase of magnetization at high fields [Fig. 3(b)]. The magnetic hysteresis loops indicate the existence of net/spontaneous magnetization. In combination with the high-field linear M-H, it suggests a canted AFM phase in both the low-temperature $(T < 7.3$ K) and intermediate-temperature $(7.3$ K $< T < 8.5$ K) regimes, as evidenced later by ESR measurement. As shown in Fig. 3(b), the remnant magnetization and coercivity at ~ 2 K (the low-temperature phase) are higher than at ~ 7.5 K (the intermediate-temperature phase), indicating that the former may have a larger canting angle than the latter (as will be discussed quantitatively below). Moreover, the M-H at ~ 2 K has clear substructures, in which the magnetization decreases abruptly as the field is reduced below 0 Oe, followed by a visible shoulder. The precise origin of this feature is not clear, but the M-H curve seems to consist of two loops with different magnetic coercivities. Therefore, it may be due to strong magnetic anisotropy at this temperature, e.g. the small crystals whose c-axis is oriented along the magnetic field direction may have

a coercivity that is strongly distinct from the crystals whose ab plane is parallel to the field. In contrast to the magnetic hysteresis loops observed at lower temperatures, the M-H curves at 10 and 15 K, namely above T_2, exactly pass through the original point. Despite the absence of hysteresis loop, these two curves are not linear. We used the field dependent magnetization equation $M = NgJ\mu_B B_J(gJ\mu_B H/k_B T)$, where the Brillouin function $B_J(x) = \frac{2J+1}{2J}\coth(\frac{(2J+1)x}{2J}) - \frac{1}{2J}\coth(\frac{x}{2J})$[44], to fit these M-H data in Fig. 3(c) and obtained the following parameters: $J = 6.03$ and 2.00 for 10 K and 15 K, respectively; the number of moments $N = 0.033\ N_{\text{Ir}}$ and $0.119\ N_{\text{Ir}}$ for 10 K and 15 K, respectively. Here N_{Ir} is the number of iridium ions, g is the Landé g-factor, and J the total angular momentum quantum number, μ_B the Bohr magneton, H the applied magnetic field, and k_B the Boltzmann constant. The large J and small N suggest that the system is unlikely to be in a conventional paramagnetic state. A possible scenario is that a short-range canted AFM ordering is established in this temperature region, and the formed 'magnetic clusters' as super-spins have larger moments (or J) than single Ir^{4+} ions ($J_{\text{eff}}=1/2$). This short-range ordering is consistent with the observation of positive magnetic heat capacity in Fig. 2(b).

ESR measurements were carried out to further understand the nature of the magnetic phases below T_2. Figure 4(a) shows the ESR spectra (i.e., first derivative of absorption with respect to field) taken at variable temperatures from 2 K to 300 K. All the spectra below T_2 show clearly three resonance peaks at $H_1 \sim 0$ Oe, $H_2 \sim 3315$ Oe, and $H_3 \sim 4278$ Oe, respectively. The intensity of the zero-field resonance increases dramatically with increase of temperature to 16 K, and then decreases upon further warming to 20 K. No clear resonance at H_2 or H_3 was observed between 10 and 20 K, which may be due to the large background signal from the resonance at zero field. Above 20 K, the resonances at $H_1 \sim 0$ Oe and $H_3 \sim 4278$ Oe both disappear, leaving only the resonance at $H_2 \sim 3315$ Oe which persists up to 300 K. The single resonance at H_2 should be attributed to the standard paramagnetic resonance in which spin of unpaired electron in a paramagnet is excited when the microwave energy and Zeeman energy equal. The Landé g-factor of the unpaired electron can then be calculated based on the equation $h\nu = g\mu_B H_r$, where h is the Planck constant, ν the microwave frequency and H_r the resonant field. The calculated g value of ~ 2.025 is slightly higher than that for a free electron ($g_{\text{e}} = 2.002$).

The resonances at H_1 ($<H_2$) and H_3 ($>H_2$) are attributed to antiferromagnetic resonance (AFMR) that occurs in the ordered state of antiferromagnetic materials[45–52]. In brief,

5

sublattice moments in an AFM state precess in the presence of both the effective internal magnetic field and the applied magnetic field. A resonant absorption occurs when the frequency of the applied excitation source equals the frequency of precession. The resonant frequency or field depends on the direction of the applied magnetic field with respect to the magnetic principle axes of the sample. In a polycrystalline sample where all orientations are possible, both the perpendicular mode (i.e., magnetic easy axis is perpendicular to external field H_0) and the parallel mode (i.e., easy axis is parallel to H_0) can be observed in the spectra. We note that the zero-field resonance frequency in our sample is about 20 times lower than that in Sr_2IrO_4[26], which should be attributed to the much weaker exchange interactions in the double-perovskite lattice. Indeed the Ir^{4+} are well separated in La_2ZnIrO_6 and the magnetic ordering temperatures are ~ 20 times lower than that in Sr_2IrO_4[25]. The observation of AFMR strongly suggests that La_2ZnIrO_6 has an AFM structure. Given the large FM component observed in the M-H measurement, the magnetic state below $T_2 \sim$ 8.5 K should be attributed to a canted AFM. The origin of the dramatic enhancement of zero-field resonance (i.e., increased amplitude and width) between 10 K and 20 K is unclear. However, it seems to correlate qualitatively with the magnetization and heat capacity data which suggest a possible short-range magnetic ordering in this temperature regime. We note that short range AFM ordering was found to persist well above Néel temperatures in the prototypical AFM systems such as MnO and NiO[53,54]. This was attributed to the frustration of spins in the face-centered-cubic (FCC) lattice[54]. The Ir^{4+} ions form a quasi-FCC lattice in La_2ZnIrO_6, therefore some frustration may also exist, as observed in some other $5d$ double perovskite compounds[55,56]. It is possible that the zero-field resonance frequency matches with the microwave frequency in the short-range ordered state and it deviates slightly when the temperature is decreased[50,57], leading to a suppression of signal. Frequency dependent AFMR measurements will be carried out in the near future to verify this scenario.

We now estimate the canting angle of the Ir^{4+} moment in the canted AFM states. The J_{eff}=1/2 Ir^{4+} has a magnetic moment of 1 μ_B in the ionic limit[1], but the local moment at each Ir site in iridates is usually less than 1 μ_B due to its hybridization with the neighboring oxygen orbits[1,39,58]. Recent density functional theory calculations suggest that the local moment of Ir^{4+} in double perovskite La_2ZnIrO_6 is ~ 0.55 μ_B for an on-site Coulomb repulsion $U \sim 1$ eV[39]. Using this value and the remanent magnetization in the M-H data at 2 K and 7.5 K, we estimated the canting angle for the low temperature phase ($T < 7.3$ K) and

6

the intermediate temperature phase (7.3 K $\leq T < 8.5$ K) to be $36°$ and $11°$, respectively. Such large canting angles can be understood by a simple model that includes the Heisenberg exchange interaction and the Dzyaloshinskii-Moriya (DM) interaction. While the Heisenberg interaction tends to align the neighboring moments collinearly, the DM interaction, which appears as a cross product of a pair of spins, prefers the neighboring moments to be perpendicular[8,59,60]. Since recent DFT calculations[39] have suggested that the moments are nearly in the xy plane of the crystal, we assume an anisotropic DM interaction and write down the interaction Hamiltonian as

$$\mathcal{H} = \sum_{<i.j>} \left[-I\vec{S}_i \cdot \vec{S}_j + D(S_{i,\mathbf{x}}S_{j,\mathbf{y}} - S_{i,\mathbf{y}}S_{j,\mathbf{x}}) \right] , \tag{1}$$

in which $I < 0$ represents the isotropic Heisenberg antiferromagnetic coupling and D the DM interaction between Ir^{4+} moments in different xy planes. We note that the DM interaction can indeed exist between these moments, given the lack of inversion symmetry at their middle point. The ground state energy can then be determined as $-D\sin 2\theta - |I|\cos 2\theta$ and minimizing the energy gives rise to a canting angle $\theta \sim \frac{1}{2}\tan^{-1}\frac{D}{|I|}$[58,61]. The large canting angle is hence attributed to the strong DM interaction with respect to isotropic AFM coupling.

We now estimate $|I|$ and D by fitting the non-linear temperature dependent inverse-susceptibility data using a modified Curie-Weiss law. In the mean-field level of equation (1), the magnetization in a paramagnetic state with a magnetic field along x-direction can be calculated using the following equations,

$$M_{1x} = \frac{C}{T}(H - \lambda_I M_{2x} - \lambda_D M_{2y}) , \tag{2}$$

$$M_{1y} = -\frac{C}{T}(\lambda_I M_{2y} - \lambda_D M_{2x}) , \tag{3}$$

$$M_{2x} = \frac{C}{T}(H - \lambda_I M_{1x} + \lambda_D M_{1y}) , \tag{4}$$

$$M_{2y} = -\frac{C}{T}(\lambda_I M_{1y} + \lambda_D M_{1x}) . \tag{5}$$

Here M_{1x} (or M_{2x}) and M_{1y} (or M_{2y}) are the magnetization by sublattice 1 (or 2) in x and y directions, respectively; $C = N\mu_{\text{eff}}^2/6k_B$ is the Curie constant for a single sublattice and μ_{eff} is the effective moment; λ_I and λ_D are the constants relating magnetization to the local exchange field in the mean field approximation for the Heisenberg and DM interactions, respectively. The total magnetization in the direction of magnetic field is $M_x = M_{1x} + M_{2x}$

7

and the magnetic susceptibility $\chi_x = dM_x/dH$ as a function of temperature is

$$\frac{1}{\chi_x} = \frac{1}{2C}[(T + \Theta_I) - \frac{\Theta_D^2}{T - \Theta_I}] \,, \tag{6}$$

in which the two temperature scales $\Theta_I = \lambda_I C$ and $\Theta_D = \lambda_D C$. The first term on the right side of equation (6) corresponds to the ordinary Curie-Weiss law in antiferromagnetic materials, while the second term arising from the DM interaction is responsible for the deviation from the linear temperature dependence of $1/\chi$ (see Fig. S2 in the Supplemental Material[42]). Besides, the magnetic susceptibility for z direction obeys the standard Curie-Weiss law. In order to account for magnetic susceptibility of the powder, we set $\chi = \frac{1}{3}\chi_z + \frac{2}{3}\chi_x$ to include contributions from all directions. The modified model is used to fit the inverse susceptibility in the temperature range of 50 K to 300 K (i.e., completely in PM state). The fitted curve and the experimental data in Fig. 5 agree reasonably well, given that our simple model includes interactions only between sublattices. The obtained parameters are: $\mu_{\text{eff}} = 1.66\ \mu_B$, $\Theta_I = 35$ K, and $\Theta_D = 23$ K, leading to a high ratio $D/|I| \sim 0.66$. If we assume that the interactions D and $|I|$ are nearly temperature independent, then the canting angle can be estimated as: $\theta \approx \frac{1}{2}\tan^{-1}\frac{D}{|I|} = 16.7°$, which is on the same order of magnitude as the values obtained from the analysis of M-H data.

The high $D/|I|$ ratio can be attributed to the large spatial separation (~ 5.6 Å) between Ir^{4+} ions in the double perovskite structure. In brief, the Heisenberg AFM exchange interaction $|I| \sim \frac{t^2}{U}$ can be significantly suppressed by the reduction of electron hopping t between the well separated Ir^{4+} ions. The low t is evidenced by the highly insulating behavior of La_2ZnIrO_6 whose electrical resistivity (see Fig. S3 in the Supplemental Material[42]) is higher than most of the iridiates[14,15,19,21,25,30,62–72]. The weak isotropic AFM interaction hence results in a strong ferromagnetic component ($\sim 0.33\ \mu_B$/Ir which is the largest among other iridates that have Ir^{4+} as the only magnetic ion). We note that such a 'ferromagnetic' insulator with a large net moment is rare in conventional ferromagnetic oxides in which conduction electrons are the key to mediate FM exchange interactions (e.g. double-exchange interaction). One of the exceptions for $5d$ transition metal oxides is the double pervoskite Ba_2NaOsO_6 which was demonstrated to be a ferromagnetic Mott insulator with an ordered moment of $\sim 0.2\ \mu_B$ per formula unit[73], possibly arising from the quadrupolar mechanism[74]. The La_2ZnIrO_6 represents another $5d$ metal oxide system of highly insulating and strong 'ferromagnetic' properties both arising from the large spatial separation between magnetic

ions.

B. $(La_{1-x}Sr_x)_2ZnIrO_6$ ($x = 0.1$ and $x = 0.2$) doped samples

We have further performed magnetization measurements on the 10% and 20% Sr^{2+} doped La_2ZnIrO_6 samples to study the influence of Ir^{5+} on magnetic properties. As shown in Figs. 6(a) and 6(b), both doped samples show clearly two magnetic transitions in the M-T curves. The magnetic transition temperatures determined by differential method [inset of Figs. 6(a) and 6(b)] are plotted against doping concentration in Fig. 6(c). Both T_1 and T_2 decreases with doping, indicating the weakening of magnetic interactions. The two magnetic transitions in the $x = 0.1$ sample are further confirmed by the temperature dependent heat capacity data shown in Fig. 7(a). For the $x = 0.2$ sample, the heat capacity is significantly reduced and it exhibits a broad band below 10 K, preventing an accurate determination of transition temperatures. Figure 7(b) shows the magnetic entropy for all three samples ($x = 0$, 0.1 and 0.2). Clearly the magnetic entropy decreases with Sr^{2+} doping, further confirming the weakening of magnetic interactions. The introduction of Ir^{5+} also enhances electrical conductivity although it does not change the insulating nature of the system (see Fig. S3 in the Supplemental Material[42]).

Doping of one Sr^{2+} ion changes one Ir^{4+} to Ir^{5+} with $5d^4$ configuration which is expected to be in a non-magnetic singlet spin state in the strong SOC limit. However, recent studies on double perovskite Sr_2YIrO_6 demonstrate a well-formed magnetic moment of Ir^{5+}. This is attributed to the strong non-cubic crystal fields that are comparable to or dominant over local exchange interactions and SOC[33]. It is not clear whether the same picture also applies in our system. If the SOC is dominant in Sr^{2+} doped La_2ZnIrO_6 and the Ir^{5+} is in a singlet J_{eff}=0 state, then the spatial separation between magnetic ions is increased due to the reduced density of magnetic Ir^{4+}. The nearest-neighboring exchange strength is hence suppressed, resulting in a decrease of ordering temperatures [Fig. 6(c)]. On the other hand, if the non-cubic crystal field dominates, then the Ir^{5+} is magnetic and the exchange interaction between Ir^{4+} and Ir^{5+} are expected to be different from the original Ir^{4+}-Ir^{4+} interaction. We noticed that although the magnetic susceptibility data of $x = 0$ and 0.1 samples can be fitted well using our modified Curie-Weiss law, the $x = 0.2$ deviates significantly (Fig. 5 and Fig. S4 in the Supplemental Material[42]). It is well-known that ferrimagnet which

has sublattices of different moments shows non-linear temperature dependence of inverse susceptibility. So the significantly non-linear $1/\chi$-T in $x = 0.2$ may be related to different moments between Ir^{4+} and Ir^{5+}, in addition to the DM interaction discussed above.

IV. CONCLUSIONS

In summary, we have performed a systematic study of magnetic properties of La_2ZnIrO_6 and its hole-doped compounds $(La_{1-x}Sr_x)_2ZnIrO_6$ via dc magnetization measurement, heat capacity characterization, ESR spectroscopy and simple modeling. We observed two magnetic transitions in the undoped La_2ZnIrO_6, and the corresponding magnetic phases below these transition temperatures are demonstrated to be canted AFM with different canting angles. The nature of the canted AFM and the high temperature magnetic susceptibility data can be understood by the Heisenberg exchange model plus the DM interaction. With the introduction of Ir^{5+} by Sr doping, the canted-AFM orderings are suppressed down to lower temperatures, accompanied by an enhancement of electrical conductivity. La_2ZnIrO_6 has higher electrical resistivity and stronger ferromagnetic component than most of the other iridates, and is one of the few $5d$ transition metal oxides that are 'ferromagnetic' insulators.

---

* sxzhang@indiana.edu

[1] B. J. Kim, H. Jin, S. J. Moon, J. Y. Kim, B. G. Park, C. S. Leem, J. Yu, T. W. Noh, C. Kim, S. J. Oh, J. H. Park, V. Durairaj, G. Cao and E. Rotenberg, Phys. Rev. Lett. **101**, 076402 (2008).

[2] D. Pesin and L. Balents, Nature Physics **6**, 376 (2010).

[3] B.-J. Yang and Y. B. Kim, Phys. Rev. B **82**, 085111 (2010).

[4] X. Wan, A. M. Turner, A. Vishwanath and S. Y. Savrasov, Phys. Rev. B **83**, 205101 (2011).

[5] S. Bhattacharjee, S.-S. Lee and Y. B. Kim, New J. Phys. **14**, 073015 (2012).

[6] W. Witczak-Krempa, G. Chen, Y. B. Kim and L. Balents, Annu. Rev. Condens. Matter Phys. **5**, 57 (2014).

[7] B. J. Kim, H. Ohsumi, T. Komesu, S. Sakai, T. Morita, H. Takagi and T. Arima, Science **323**, 1329 (2009).

[8] G. Jackeli and G. Khaliullin, Phys. Rev. Lett. **102**, 017205 (2009).

[9] F. Wang and T. Senthil, Phys. Rev. Lett. **106**, 136402 (2011).

[10] Y. Machida, S. Nakatsuji, S. Onoda, T. Tayama and T. Sakakibara, Nature **463**, 210 (2010).

[11] T. Dodds, T.-P. Choy and Y. B. Kim, Phys. Rev. B **84**, 104439 (2011).

[12] M. Kargarian, J. Wen and G. A. Fiete, Phys. Rev. B **83**, 165112 (2011).

[13] W. Witczak-Krempa and Y. B. Kim, Phys. Rev. B **85**, 045124 (2012).

[14] D. Yanagishima and Y. Maeno, J. Phys. Soc. Jpn. **70**, 2880 (2001).

[15] T. F. Qi, O. B. Korneta, X. Wan, L. E. DeLong, P. Schlottmann and G. Cao, J. Phys.: Condens. Matter **24**, 345601 (2012).

[16] H. Sagayama, D. Uematsu, T. Arima, K. Sugimoto, J. J. Ishikawa, E. O'Farrell and S. Nakatsuji, Phys. Rev. B **87**, 100403(R) (2013).

[17] M. Sakata, T. Kagayama, K. Shimizu, K. Matsuhira, S. Takagi, M. Wakeshima and Y. Hinatsu, Phys. Rev. B **83**, 041102(R) (2011).

[18] M. C. Shapiro, S. C. Riggs, M. B. Stone, C. R. de la Cruz, S. Chi, A. A. Podlesnyak and I. R. Fisher, Phys. Rev. B **85**, 214434 (2012).

[19] S. M. Disseler, C. Dhital, A. Amato, S. R. Giblin, C. de la Cruz, S. D. Wilson and M. J. Graf, Phys. Rev. B **86**, 014428 (2012).

[20] W. K. Zhu, M. Wang, B. Seradjeh, F. Yang and S. X. Zhang, Phys. Rev. B **90**, 054419 (2014).

[21] Y. Singh and P. Gegenwart, Phys. Rev. B **82**, 064412 (2010).

[22] S. K. Choi, R. Coldea, A. N. Kolmogorov, T. Lancaster, I. I. Mazin, S. J. Blundell, P. G. Radaelli, Y. Singh, P. Gegenwart, K. R. Choi, S. W. Cheong, P. J. Baker, C. Stock and J.

Taylor, Phys. Rev. Lett. **108**, 127204 (2012).

[23] X. Liu, T. Berlijn, W. G. Yin, W. Ku, A. Tsvelik, Y.-J. Kim, H. Gretarsson, Y. Singh, P. Gegenwart and J. P. Hill, Phys. Rev. B **83**, 220403 (2011).

[24] F. Ye, S. Chi, H. Cao, B. C. Chakoumakos, J. A. Fernandez-Baca, R. Custelcean, T. F. Qi, O. B. Korneta and G. Cao, Phys. Rev. B **85**, 180403 (2012).

[25] G. Cao, J. Bolivar, S. McCall, J. E. Crow and R. P. Guertin, Phys. Rev. B **57**, 11039 (1998).

[26] S. Bahr, A. Alfonsov, G. Jackeli, G. Khaliullin, A. Matsumoto, T. Takayama, H. Takagi, B. Büchner and V. Kataev, Phys. Rev. B **89**, 180401(R) (2014).

[27] J. Kim, D. Casa, M. H. Upton, T. Gog, Y.-J. Kim, J. F. Mitchell, M. van Veenendaal, M. Daghofer, J. van den Brink, G. Khaliullin and B. J. Kim, Phys. Rev. Lett. **108**, 177003 (2012).

[28] F. Ye, S. Chi, B. C. Chakoumakos, J. A. Fernandez-Baca, T. Qi and G. Cao, Phys. Rev. B **87**, 140406 (2013).

[29] A. V. Powell, J. G. Gore and P. D. Battle, J. Alloy. Compd. **201**, 73 (1993).

[30] E. M. Ramos, I. Alvarez, M. L. Veiga and C. Pico, Mater. Res. Bull. **29**, 881 (1994).

[31] R. C. Currie, J. F. Vente, E. Frikkee and D. J. W. Ijdo, J. Solid State Chem. **116**, 199 (1995).

[32] P. D. Battle and J. G. Gore, J. Mater. Chem. **6**, 1375 (1996).

[33] G. Cao, T. F. Qi, L. Li, J. Terzic, S. J. Yuan, L. E. DeLong, G. Murthy and R. K. Kaul, Phys. Rev. Lett. **112**, 056402 (2014).

[34] M. J. Davis, S. J. Mugavero, K. I. Glab, M. D. Smith and H. C. zur Loye, Solid State Sci. **6**, 413 (2004).

[35] P. Kayser, M. J. Martínez-Lope, J. A. Alonso, M. Retuerto, M. Croft, A. Ignatov and M. T. Fernández-Díaz, Inorg. Chem. **52**, 11013 (2013).

[36] H. Daijitsu, W. Makoto, H. Yukio, O. Kenji and Y. Yasuo, J. Phys.: Condens. Matter **12**, 3229 (2000).

[37] N. Narayanan, D. Mikhailova, A. Senyshyn, D. M. Trots, R. Laskowski, P. Blaha, K. Schwarz, H. Fuess and H. Ehrenberg, Phys. Rev. B **82**, 024403 (2010).

[38] A. Kolchinskaya, P. Komissinskiy, M. B. Yazdi, M. Vafaee, D. Mikhailova, N. Narayanan, H. Ehrenberg, F. Wilhelm, A. Rogalev and L. Alff, Phys. Rev. B **85**, 224422 (2012).

[39] G. Cao, A. Subedi, S. Calder, J. Q. Yan, J. Yi, Z. Gai, L. Poudel, D. J. Singh, M. D. Lumsden, A. D. Christianson, B. C. Sales and D. Mandrus, Phys. Rev. B **87**, 155136 (2013).

40 A. C. Larson and R. B. V. Dreele, Los Alamos National Laboratory Report LAUR 86-748 (2004).

41 B. H. Toby, J. Appl. Crystallogr. **34**, 210 (2001).

42 See Supplemental Material at [ ] for more details about X-ray diffraction, the modified model, and electrical resistivity, etc.

43 L. D. Landau and E. M. Lifshitz, *Statistical Physics 3rd Edition Part 1.* (Elsevier Ltd., 1980).

44 C. Kittel, *Introduction to Solid State Physics Eighth Edition.* (John Wiley & Sons, Inc, United States of America, 2005).

45 T. Nagamiya, Prog. Theor. Phys. **11**, 309 (1954).

46 J. B. Torrance, H. J. Pedersen and K. Bechgaard, Phys. Rev. Lett. **49**, 881 (1982).

47 K. Katsumata and J. Tuchendler, J. Phys. C: Solid State Phys. **20**, 4873 (1987).

48 E. W. Ong, G. H. Kwei, R. A. Robinson, B. L. Ramakrishna and R. B. Von Dreele, Phys. Rev. B **42**, 4255 (1990).

49 H. Ohta, K. Yoshida, T. Matsuya, T. Nanba, M. Motokawa, K. Yamada, Y. Endoh and S. Hosoya, J. Phys. Soc. Jpn. **61**, 2921 (1992).

50 H. Ohta, N. Yamauchi, T. Nanba, M. Motokawa, S. Kawamata and K. Okuda, J. Phys. Soc. Jpn. **62**, 785 (1993).

51 M. Hagiwara, K. Katsumata and J. Tuchendler, J. Phys.: Condens. Matter **6**, 545 (1994).

52 G. E. Fanucci, J. Krzystek, M. W. Meisel, L. C. Brunel and D. R. Talham, J. Am. Chem. Soc. **120**, 5469 (1998).

53 A. Renninger, S. Moss and B. Averbach, Phys. Rev. **147**, 418 (1966).

54 T. Chatterji, G. J. McIntyre and P. A. Lindgard, Phys. Rev. B **79**, 172403 (2009).

55 T. Aharen, J. E. Greedan, C. A. Bridges, A. A. Aczel, J. Rodriguez, G. MacDougall, G. M. Luke, V. K. Michaelis, S. Kroeker, C. R. Wiebe, H. Zhou and L. M. D. Cranswick, Phys. Rev. B **81**, 064436 (2010).

56 A. A. Aczel, P. J. Baker, D. E. Bugaris, J. Yeon, H. C. zur Loye, T. Guidi and D. T. Adroja, Phys. Rev. Lett. **112**, 117603 (2014).

57 M. Y. Ruan, Z. W. Ouyang, Y. M. Guo, J. J. Cheng, Y. C. Sun, Z. C. Xia, G. H. Rao, S. Okubo and H. Ohta, J. Phys.: Condens. Matter **26**, 236001 (2014).

58 H. Jin, H. Jeong, T. Ozaki and J. Yu, Phys. Rev. B **80**, 075112 (2009).

59 I. Dzyaloshinsky, J. Phys. Chem. Solids **4**, 241 (1958).

[60] T. Moriya, Phys. Rev. 120, 91 (1960).

[61] G. F. Herrmann, J. Phys. Chem. Solids **24**, 597 (1963).

[62] S. Nagata, T. Hagino, Y. Seki and T. Bitoh, Physica B **194-196**, 1077 (1994).

[63] P. D. Battle, G. R. Blake, T. C. Gibb and J. F. Vente, J. Solid State Chem. **145**, 541 (1999).

[64] K. Matsuhira, M. Wakeshima, Y. Hinatsu and S. Takagi, J. Phys. Soc. Jpn. **80**, 094701 (2011).

[65] J.-H. Chu, S. C. Riggs, M. Shapiro, J. Liu, C. R. Serero, D. Yi, M. Melissa, S. J. Suresha, C. Frontera, A. Vishwanath, X. Marti, I. R. Fisher and R. Ramesh, arXiv **1309.4750v2** (2013).

[66] J. J. Ishikawa, E. C. T. O'Farrell and S. Nakatsuji, Phys. Rev. B **85**, 245109 (2012).

[67] W. Ryden, A. Lawson and C. Sartain, Phys. Rev. B **1**, 1494 (1970).

[68] S. M. Disseler, C. Dhital, T. C. Hogan, A. Amato, S. R. Giblin, C. de la Cruz, A. Daoud-Aladine, S. D. Wilson and M. J. Graf, Phys. Rev. B **85**, 174441 (2012).

[69] K. Ueda, J. Fujioka, Y. Takahashi, T. Suzuki, S. Ishiwata, Y. Taguchi and Y. Tokura, Phys. Rev. Lett. **109**, 136402 (2012).

[70] H. Fukazawa and Y. Maeno, J. Phys. Soc. Jpn. **71**, 2578 (2002).

[71] G. Cao, V. Durairaj, S. Chikara, L. E. DeLong, S. Parkin and P. Schlottmann, Phys. Rev. B **76**, 100402(R) (2007).

[72] G. Cao, J. E. Crow, R. P. Guertin, P. F. Henning, C. C. Homes, M. Strongin, D. N. Basov and E. Lochner, Solid State Commun. **113**, 657 (2000).

[73] A. S. Erickson, S. Misra, G. J. Miller, R. R. Gupta, Z. Schlesinger, W. A. Harrison, J. M. Kim and I. R. Fisher, Phys. Rev. Lett. **99**, 016404 (2007).

[74] G. Chen, R. Pereira and L. Balents, Phys. Rev. B **82**, 174440 (2010).
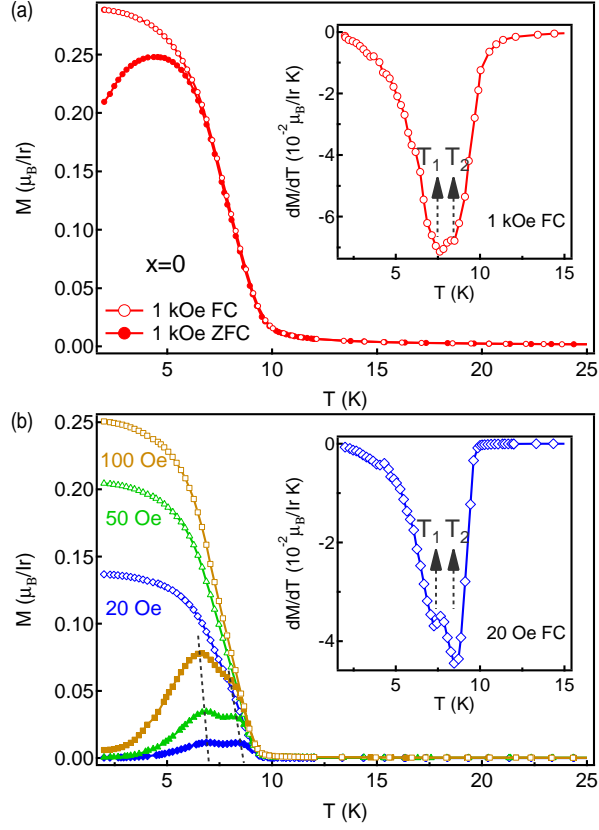
FIG. 1. Temperature dependence of ZFC (solid) and FC (open) magnetizations taken on the undoped La_2ZnIrO_6 at (a) 1 kOe and (b) lower fields (100, 50 and 20 Oe). The dashed lines in (b) indicate the increase of peak temperatures with the decrease of magnetic field. The insets show the derivative of magnetization with respect to temperature. The dashed arrows indicate transition temperatures T_1 and T_2.
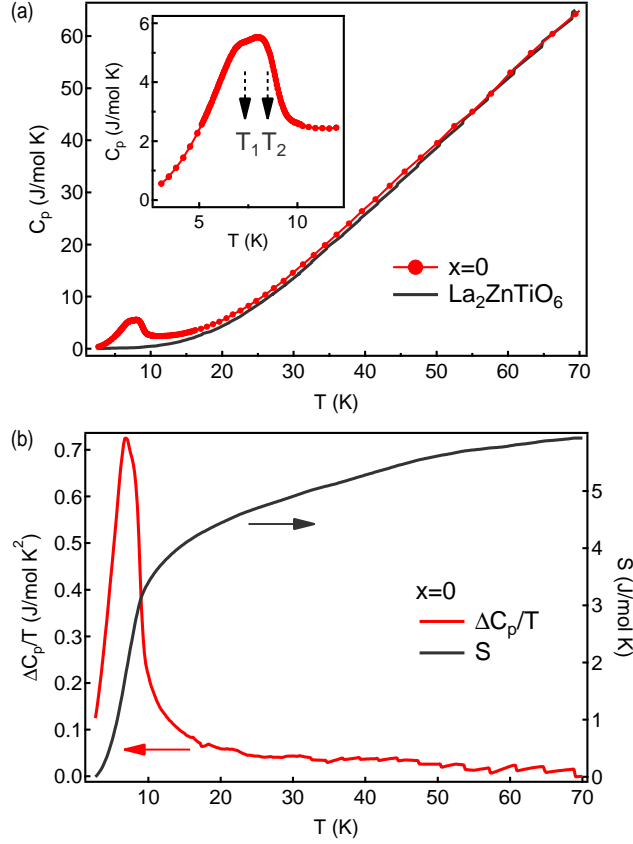
FIG. 2. (a) Temperature dependence of specific heat C_p of La_2ZnIrO_6 and La_2ZnTiO_6. The latter was scaled at 70 K to represent the lattice specific heat of the former. The inset shows the specific heat of La_2ZnIrO_6 at low temperatures and the dashed arrows indicate the two magnetic transition temperatures T_1 and T_2. (b) The magnetic specific heat ΔC_p and the magnetic entropy S of La_2ZnIrO_6 as a function of temperature. Interpolation was applied when subtracting two specific heat data due to their different temperature steps.
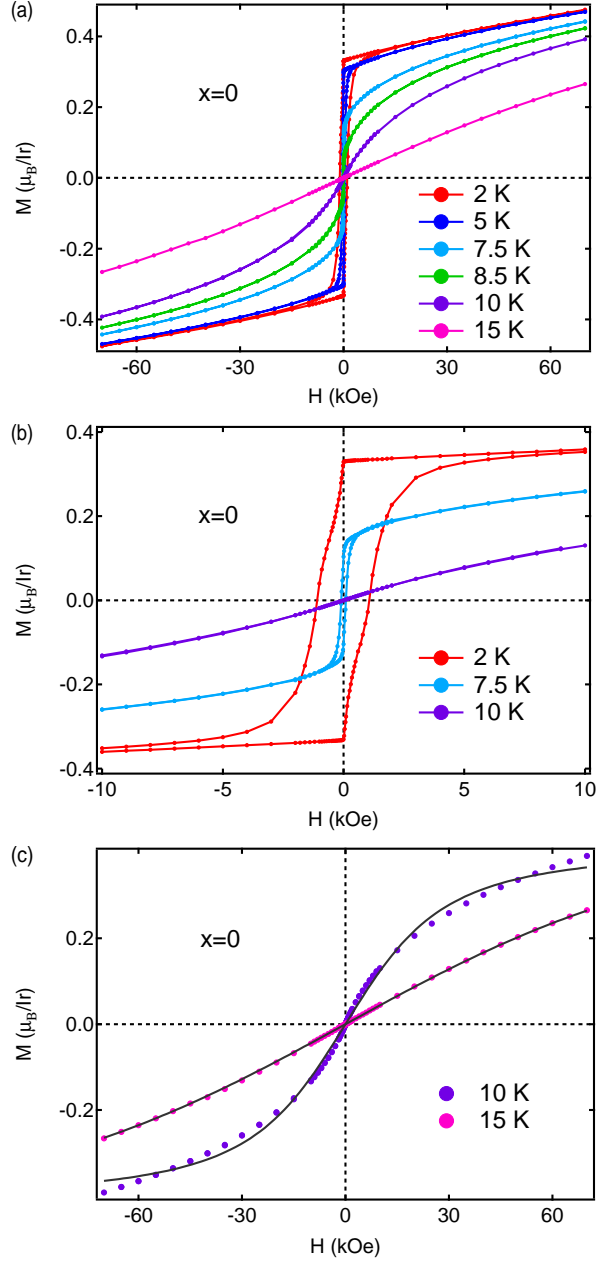
FIG. 3. (a) M-H data of La$_2$ZnIrO$_6$ taken at several temperatures in a field range of -70 kOe to 70 kOe. (b) M-H curves in a field range of -10 kOe to 10 kOe showing hysteresis loops at 2 K and 7.5 K, and absence of loop at 10 K. (c) Fitting of the M-H data at 10 and 15 K using the Brillouin function. The dots are experimental data and the solid curves are fitting data.
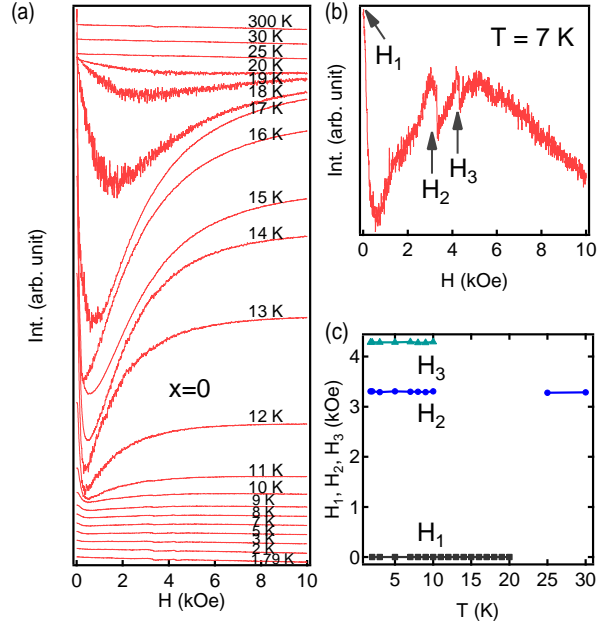
FIG. 4. (a) ESR spectra of La_2ZnIrO_6 taken at different temperatures from 1.79 K to 300 K. The spectra are shifted vertically for clarity. (b) A typical ESR spectrum below T_2 showing three resonant peaks. (c) The resonant fields H_1, H_2 and H_3 as a function of temperature.
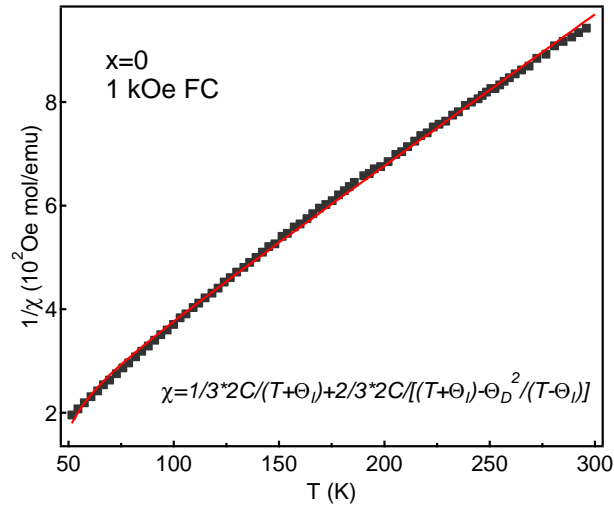
FIG. 5. Temperature dependent inverse susceptibility data of La_2ZnIrO_6 in the paramagnetic state. The black squares are experimental data and the red curve is the fitting data using the modified Curie-Weiss model.

18
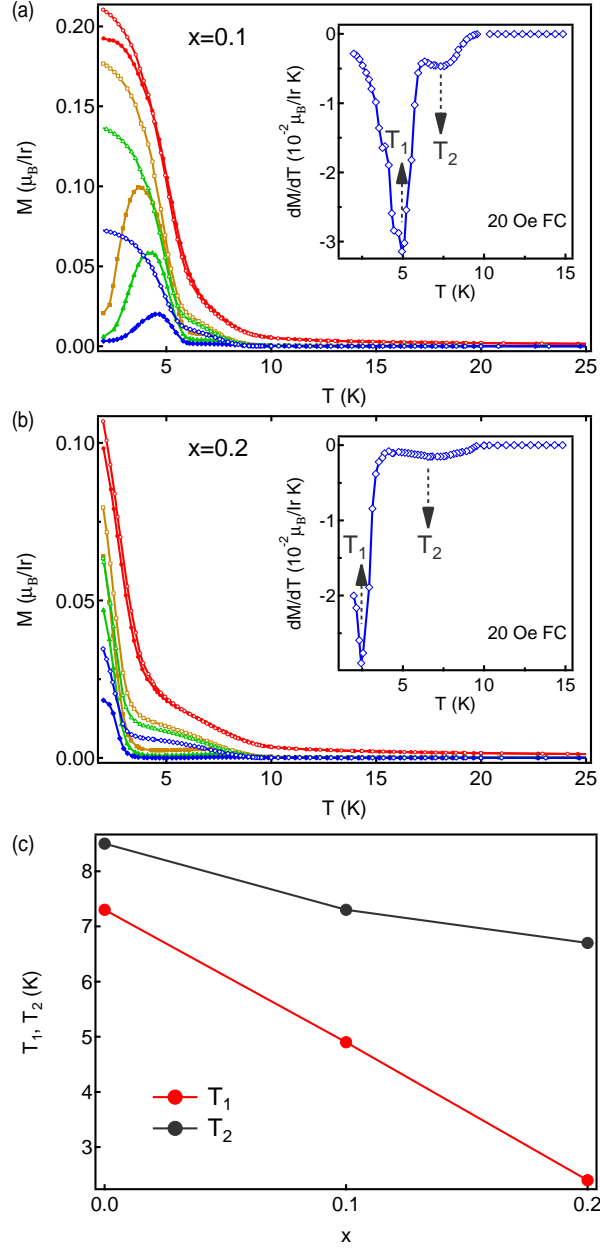
FIG. 6. Temperature dependence of ZFC (solid) and FC (open) magnetizations taken on (a) $x = 0.1$ and (b) $x = 0.2$ samples at different magnetic fields (1 kOe: red circles; 100 Oe: yellow squares; 50 Oe: green triangles and 20 Oe: blue diamonds). The insets show the derivative of magnetization with respect to temperature taken at 20 Oe. The dashed arrows indicate transition temperatures T_1 and T_2. (c) The transition temperatures as a function of doping concentration x.
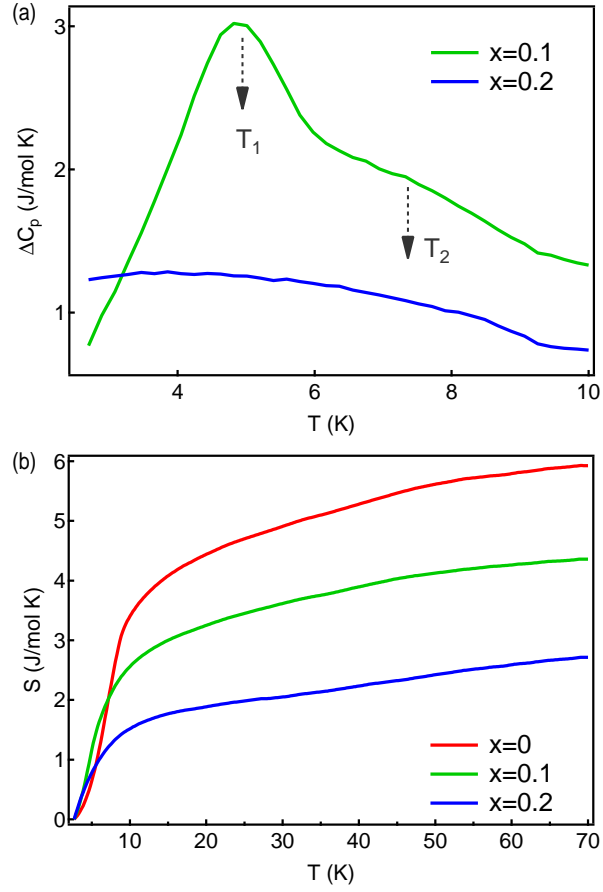
FIG. 7. (a) Temperature dependence of magnetic specific heat ΔC_p of $x = 0.1$ and 0.2 samples. (b) A comparison of magnetic entropy S for all three samples.